Angular differential cross sections for 25-, 50-, and 100-keV-proton excitation of helium to the $n = 2$ level

J. T. Park, J. M. George, J. L. Peacher, and J. E. Aldag

Physics Department, University of Missouri at Rolla, Rolla, Missouri 65401

Differential cross sections for 25-, 50-, and 100-keV-proton excitation of helium to the $n = 2$ level have been determined for center-of-mass scattering angles from 0 to 1.2 mrad. The cross sections were obtained from an analysis of the angular distribution of the scattered protons which had lost an energy corresponding to the excitation of the helium target to its $n = 2$ level. The differential cross section is very sharply peaked in the forward direction and decreases by a factor of 45 in 1.0 mrad at 25 keV and by a factor of 650 in 1.0 mrad at 100 keV. The data are in excellent agreement with a recent multistate eikonal calculation.

I. INTRODUCTION

Recently completed modifications to the ion energy-loss spectrometer in the Department of Physics at the University of Missouri at Rolla (UMR) permit the measurement of ion-atom inelastic cross sections that are differential in both energy loss and projectile scattering angle. Earlier measurements of differential cross sections using the energy-loss spectrometer involved a different technique.[1-4] The improved apparatus and technique has resulted in higher angular resolution which permits studies of the most basic ion-atom collisional systems.

The present study concentrates on the excitation of helium to its lowest excited level by 25-, 50-, and 100-keV protons. This simple collision involves a structureless projectile colliding with a two-electron target. Only two total cross-section measurements in this general ion energy range are available for proton collisional excitation of the $n = 2$ level of helium. The work of Park and Schowengerdt[5] using energy-loss spectrometry has been extended to higher ion energy by Hippler and Schartner[6] using optical techniques. Unfortunately, the measurements do not overlap. Calculated values for the total cross section employing a wide range of different theoretical techniques are available. The present project will extend the earlier, total-cross-section work to provide angular differential cross sections for excitation of the helium target to the $n = 2$ level. These results are integrated over scattering angle to provide total cross sections for this excitation process. Calculations of differential cross sections employing Born and multistate eikonal approximations are available and theoretical studies using other approximations are feasible.

II. EXPERIMENTAL METHOD

The UMR energy-loss spectrometer and the general method employed in ion energy-loss spectrometry have been discussed in detail elsewhere[1-5,7-9]; however, the method and apparatus now in use differ in several respects from that reported earlier. The most marked change in the apparatus involves the ability to rotate the entire accelerator and beam-conditioning apparatus about the collision point. See Fig. 1. The collision chamber, accelerating column, accelerator cabinet, and cables are rotated as a unit about an axis that passes through the collision point. This technique avoids stressing any components that are critical for determining the ion-beam angle. The required flexing is accomplished on the decelerator–detector side of the collision chamber through the use of bellows and cables chosen for their flexibility.

The items composing the ion accelerator, are mounted on a heavy steel framework, which provides a solid and stable platform. The frame is pivoted on a precision 7.3-cm-diam loaded bearing. The bearing is mounted on a 61 × 91.4-cm steel plate 2.54-cm thick which is bolted and cemented to the concrete floor. The accelerator end of the framework is supported by precision ball rollers. The ball rollers are located 3.05 m from each other and 3.35 m from the pivot point. Each roller moves along a smooth machined surface on a 2.54-cm-thick steel plate bolted and cemented to the concrete floor and leveled to within an angle of 4.2×10^{-5} rad. The framework is rotated by a tangentially mounted precision screw assembly. The screw is turned by a stepping motor, which may be controlled either manually or by a computer.
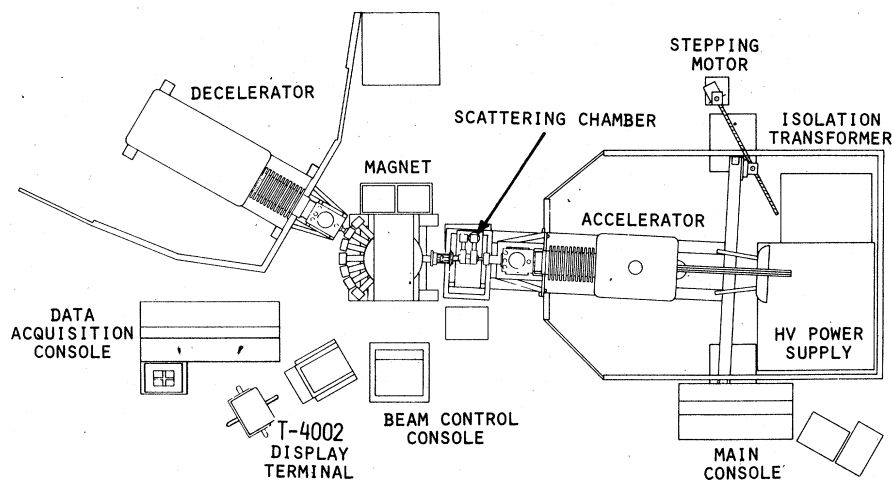
A variable-angle differentially pumped collision

48

FIG. 1. The UMR ion energy-loss spectrometer.

chamber is used for differential cross-section measurements. The chamber is designed so that the bending axis of its gas-containment bellows is the same as the axis of rotation. The pressure in the target chamber is measured by a MKS 77-1 differential manometer. The target gas is introduced into the target chamber by means of a servo-controlled valve. An automatic pressure regulator maintains the chamber pressure using the Baratron pressure meter as a reference. Pressure differences from the setting on the Baratron pressure meter can be confined to within 1% of the desired pressure. The magnitude of the actual pressure is digitally recorded with each data measurement.

Ions are produced in a low-voltage discharge source. The ion source presently in use is a Colutron G2 ion gun. The energy distribution produced by this source is estimated to have a 0.2 eV full width at half maximum (FWHM). The source is differentially pumped to prevent the ion-source gas from entering the accelerator column. Great care is exercised in the operation of the source to obtain an ion beam that has a narrow energy distribution, long-term stability, low gas consumption, and a reasonable source life. The ion gun includes a Wein filter, which is employed to permit mass selection prior to acceleration.

The mass-selected ions are accelerated and steered through the entrance collimator. The collimators and slit locations are shown schematically in Fig. 2. The collimator slits can be precisely moved in and out of the beam. This makes it possible to focus the beam at the center of the collision chamber before introducing the collimator slits. This method provides maximum beam intensity and also aids in data analysis. Additional collimating slits define the angular extent of the beam entering the collision chamber. The gas containment apertures of the collision chamber
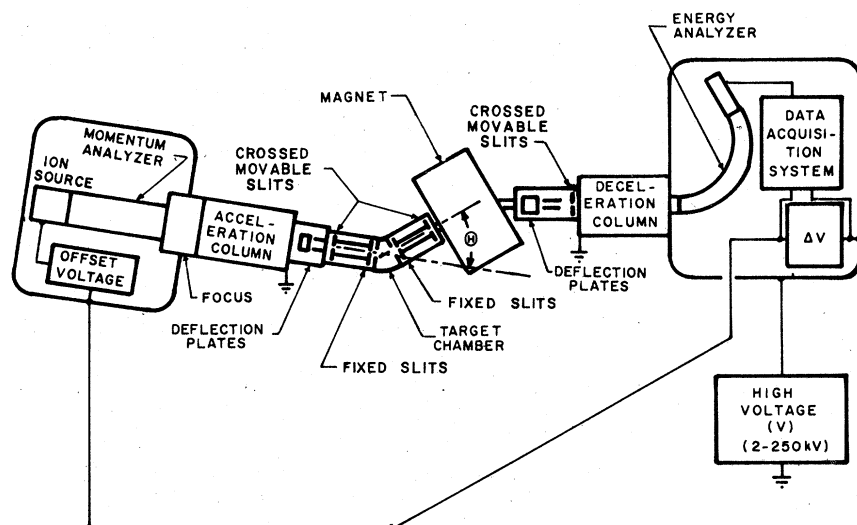

FIG. 2. Schematic drawing of the apparatus.

itself are larger than the maximum extent of the collimated beam and hence do not enter into the analysis of the collision geometry.

Ions exiting from the collision chamber pass through the exit collimator, which consists of a fixed exit slit and a pair of movable collimating slits. These slits are aligned for maximum transmission at zero scattering angle and define the detection window used in the data analysis.

The transmitted ion beam is magnetically analyzed to remove any products of charge-changing collisions. This removes any ambiguity as to the detected ion. Following the magnetic analysis, the ions enter the decelerating column and are decelerated to a well-defined potential. The decelerated ions are energy analyzed by an electrostatic analyzer.

Two techniques are used to obtain data using the modified apparatus. At a fixed scattering angle and for total cross section measurements, spectra differential in energy loss are obtained by increasing ΔV, the potential difference between the accelerator and decelerator terminals. Whenever the increased potential energy compensates for a discrete energy loss of the projectile-target system, a peak is detected in the energy-loss spectrum. The energy-loss scale can be determined to an accuracy of ± 0.03 eV.[8] Angular distributions of the scattered ion current corresponding to a particular scattering process can be measured by fixing the energy loss of interest while pivoting about the scattering center provided that the process is resolved in its energy-loss spectrum. The relative angular position of the accelerator is known to within 3.3×10^{-6} rad.

In either mode of data acquisition, the laboratory energy loss must include the kinematic effects of the recoiling target atom. Analytically, if an excitation process involves an internal excitation energy η the energy loss at a scattering angle θ is given in laboratory coordinates by

$$\Delta \xi(\theta) = \frac{2Em}{(m+M)^2} \left[M + m \sin^2\theta + \frac{M(m+M)\eta}{2mE} \right.$$

$$- \cos\theta \left(M^2 - m^2 \sin^2\theta \right.$$

$$\left. \left. - \frac{M(m+M)\eta}{E} \right)^{1/2} \right], \quad (1)$$

in which m is the mass of the projectile ion, M the mass of the target atom, and E the energy of the incident ion.

Because of the complexity of the measurement and the magnitude of data required to produce meaningful results, a minicomputer controls the data-acquisition process. The measurement scat-

tering angle, recoil-corrected energy loss, count time, and various emergency and reset signals are set and monitored by the minicomputer. Because the computer can vary the measurement time with the observed count rate, little time is wasted on measurements for which the signal-to-noise ratio is high. The transmitted ion current, energy loss, scattering angle, and scattering chamber pressure are recorded for each measurement. This information is channeled directly to or preset by the minicomputer which corrects the measurement for scattering-chamber-pressure deviations, instrument and residual gas-caused background, and normal incident-beam drift. A standard deviation is calculated for each data point and the results are averaged, background corrected, compacted and stored for further analysis.

III. DATA ANALYSIS

The results presented here were extracted from data taken by the second acquisition method. For these angular acquisitions, measurement of the angular distribution of the incident and elastically scattered beam current and of several background corrected inelastically scattered current distributions comprise a sequence of angular data which contain enough information to allow extraction of absolute angular differential cross sections. An apparent differential cross section for the process is given as in earlier work[1-4] as

$$\frac{ds_p(\theta)}{d\Omega} = \frac{I_p(\theta)}{nl\Delta\Omega(I_0)_f}. \quad (2)$$

In this expression, $I_p(\theta)$ is the singly charged particle current corresponding to the process p which is scattered into the solid detection angle $\Delta\Omega$ centered at the scattering angle θ. The term nl is the target density in units of cm^{-2}. The term $(I_0)_f$ is the total elastically scattered beam. The use of $(I_0)_f$ in place of the total incident beam exactly corrects the inelastic measurements for beam loss due to charge-changing collisions.[1] The energy-loss aspect of the apparatus allows the measurement of angular current distributions corresponding to the inelastic process of interest p. In the present case, p represents the process H^+ + He $\rightarrow$ H$^+(\theta)$ + He$^*(n=2)$. The term $ds_p(\theta)/d\Omega$ is labeled as an apparent differential cross section because it is averaged over the acceptance solid angle $\Delta\Omega$ of the detection window and the angular width of the incident beam.

To evaluate the effect of this averaging, the apparent differential cross section is analytically related to the real differential cross section for the process of interest $d\sigma_p(\theta)/d\Omega$. The resulting integral expression for $ds_p(\theta)/d\Omega$ allows the numer-
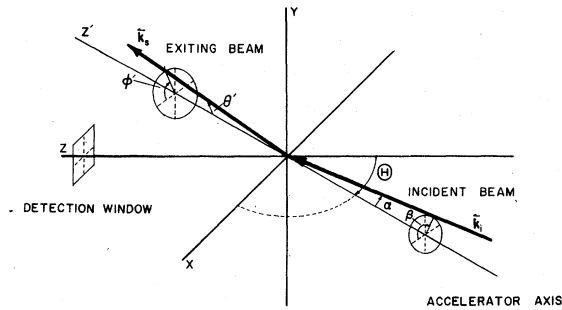
FIG. 3. Schematic drawing of the incident and scattered beams.

ical extraction of $d\sigma_p(\theta)/d\Omega$. The following assumptions are made to allow an analytical formulation of the $ds_p(\theta)/d\Omega$ as measured by the UMR angular energy-loss spectrometer. They are based on the mechanical design of the apparatus and parameters measurable during data acquisition.

(i) The incident beam is cylindrically symmetric about the accelerator-column axis and focused on the center of the scattering region. Figure 3 illustrates the assumed form of the incident-beam distribution and the parameters used to describe it. Analytically, it is expressed as $dI(\alpha)/d\Omega$. The angles α and β define the direction of the incident beam element with respect to the accelerator axis system. The angles (θ', ϕ') describe the distribution of the beam leaving the scattering region with respect to the accelerator axis system.

(ii) The scattering takes place under single-collision conditions.

(iii) The scattering occurs at the focal point of the incident beam. This allows all coordinates to be defined about a common origin and justifiably ignores the variation in the detection-window width as seen from various locations in the scattering region.

(iv) All ions passing through the detection window are detected by the decelerator analyzer system with equal efficiency.

(v) The differential cross section for the process of interest has cylindrical symmetry and is therefore written as $d\sigma_p(\theta)/d\Omega$. All of these assumptions are justified and are consistent with the design of the apparatus and the technique of data acquisition.

While the real $dI/d\Omega$ and the measured ion-beam distribution $I_{IN}(\Theta)$ are in practice only slightly different, they are not equivalent since the $I_{IN}(\Theta)$ is a convolution of $dI/d\Omega$ with the detection geometry. In the case of $dI/d\Omega$, the incident and exiting angles are equal and, at a particular measurement angle Θ, $I_{IN}(\Theta)$ is found by simply integrating $dI/d\Omega$ over the detection window:

$$I_{IN}(\Theta) = \frac{1}{R^2} \int_{\Delta x} \int_{\Delta y} \frac{dI}{d\Omega}(\theta')\, dx\, dy , \tag{3}$$

where Δx and Δy represent the width and height of the detection window and R is the distance from the scattering center to the detection window. The angle θ' is related to (x,y) and Θ by a linear coordinate transformation which rotates the unprimed system into the primed about the y axis by the angle Θ. This rotation describes the physical motion of the accelerator during data acquisition because the z' axis lies in the xz plane. Equation (3) contains $dI/d\Omega$, which must be extracted for use in an analytical representation of the $ds_p/d\Omega$.

Figure 3 illustrates the various coordinate systems used in the scattered-beam distribution model. We consider first the scattering as viewed from the accelerator axis or primed system. We consider the current scattered from the incident-beam distribution to the angles (θ', ϕ') by the scattering process p. The current scattered to (θ', ϕ'), $dI_p/d\Omega$ will contain contributions from incident-beam elements entering the scattering region at angles (α, β) and scattered through some angles (θ, ϕ) such that the beam element exits the scattering region at angles (θ', ϕ').

Analytically,

$$\frac{dI_p}{d\Omega}(\theta') = nl \int_0^{2\pi} \int_0^{\pi} \frac{dI}{d\Omega}(\alpha) \frac{d\sigma_p}{d\Omega}(\theta) \sin\alpha\, d\alpha\, d\beta. \tag{4}$$

Although θ is an explicit function of α, β, θ', and ϕ', the cylindrical symmetry of $dI/d\Omega$ and $d\sigma/d\Omega$ will result in a cylindrically symmetric scattered-beam distribution $dI_p(\theta')/d\Omega$ in the primed system. The relation between (θ', ϕ') and the angles (α, β) and θ is deduced from the dot product of the incident-beam element vector $\hat{k}_I$ and the exiting-beam element vector $\hat{k}_s$.

The dot product of the unit vectors $\hat{k}_I$ and $\hat{k}_s$ gives

$$\cos\theta = \hat{k}_I \cdot \hat{k}_s = \sin\alpha \sin\theta' \cos(\beta - \phi')$$

$$+ \cos\alpha \cos\theta'. \tag{5}$$

The portion of this scattered current distribution seen by the detection window at a particular measurement angle Θ is given by the integration of Eq. (4) over the detection window, and, as in the analytical expression for $I_{IN}(\Theta)$, the θ' is related to (x,y) and Θ by the linear coordinate transformation previously described.

By substitution of Eq. (5) into Eq. (4) and substitution of θ' in terms of x,y and Θ, and integration over the detection window, we obtain

$$I_p(\Theta) = \frac{nl}{R^2} \int_{\Delta x} \int_{\Delta y} \int_0^{2\pi} \int_0^{\pi} \frac{dI}{d\Omega}(\alpha) \frac{d\sigma_p}{d\Omega} [\theta(\alpha,\beta,x,y,\Theta)]$$

$$\times \sin\alpha \, d\alpha \, d\beta \, dx \, dy. \qquad (6)$$

Division by $nl \, \Delta\Omega$ and the total elastically scattered beam current $(I_0)_f$ results in an integral representation for the apparent angular differential cross section, $ds_p/d\Omega$; that is,

$$\frac{ds_p}{d\Omega}(\Theta) = \frac{I_p(\Theta)}{nl(I_0)_f \Delta\Omega}$$

$$= \frac{1}{\Delta x \Delta y} \int_{\Delta x} \int_{\Delta y} \int_0^{2\pi} \int_0^{\pi} \frac{1}{(I_0)_f} \frac{dI}{d\Omega}(\alpha)$$

$$\times \frac{d\sigma_p}{d\Omega}[\theta(\alpha,\beta,x,y,\Theta]$$

$$\times \sin\alpha \, d\alpha \, d\beta \, dx \, dy, \qquad (7)$$

since $\Delta\Omega = \Delta x \, \Delta y / R^2$.

Equation (7) contains the real angular differential cross section $d\sigma/d\Omega$ for the process p. Determination of $d\sigma_p/d\Omega$ from Eq. (7) requires a knowledge of $dI/d\Omega$ which must be extracted from the integral representation of $I_{IN}(\Theta)$, Eq. (3). The same numerical method is used to extract $d\sigma_p/d\Omega$ from Eq. (7) and $dI/d\Omega$ from Eq. (3). The method will be discussed in the context of $d\sigma_p/d\Omega$ but is equally applicable in the case of Eq. (3).

The numerical method extracts $d\sigma_p/d\Omega$ by equating the measured $ds_p/d\Omega$ to its integral representation at each acquisition angle with an assumed form for $d\sigma_p/d\Omega$. The assumed form for $d\sigma_p/d\Omega$ and the key assumption of the numerical extraction method is

$$\frac{d\sigma_p(\theta)}{d\Omega} = f(\theta) \frac{ds_p(\theta)}{d\Omega}, \qquad (8)$$

where $f(\theta)$ is a slowly varying apparatus-beam function of θ only and can be accurately approximated by a truncated Taylor-series expansion. This assumption reduces the problem from extraction of $d\sigma_p/d\Omega$, which may vary several orders of magnitude over the measurement range, to extraction of the function $f(\theta)$, which has a value near 1 for all angles.

We specify a particular measurement angle Θ_m. Then $m = 1$ to M specify the M data points of an angular spectra measurement. We introduce the notation

$$\theta_m = \theta(\alpha,\beta,x,y,\Theta_m). \qquad (9)$$

Since $f(\theta)$ is a slowly varying function of θ we expand $f(\theta_m)$ in a Taylor series about Θ_m and truncate the series after N terms. That is,

$$f(\theta_m) \cong \sum_{n=0}^{N-1} f_n(\Theta_m) \frac{(\theta_m - \Theta_m)^n}{n!}, \quad m = 1, M, \qquad (10)$$

with

$$f_n(\Theta_m) = \frac{d^n f(\Theta_m)}{d\theta_m^n} \Big|_{\Theta_m}. \qquad (11)$$

With the notation

$$S_n(\Theta_m) = \frac{1}{\Delta x \Delta y} \int_{\Delta x} \int_{\Delta y} \int_0^{2\pi} \int_0^{\pi} \left(\frac{1}{(I_0)_f} \frac{dI}{d\Omega}(\alpha) \right)$$

$$\times \frac{(\theta_m - \Theta_m)^n}{n!} \frac{ds_p}{d\Omega}(\theta_m)$$

$$\times \sin\alpha \, d\alpha \, d\beta \, dx \, dy, \qquad (12)$$

Eq. (7) is written as

$$\frac{ds_p}{d\Omega}(\Theta_m) = \sum_{n=0}^{N-1} f_n(\Theta_m) S_n(\Theta_m), \quad m = 1, M. \qquad (13)$$

Using the notation

$$_{m+j}\delta_m^n = \frac{(\Theta_{m+j} - \Theta_m)^n}{n!}, \qquad (14)$$

auxiliary equations of the form

$$f_0(\Theta_{m+j}) = f_0(\Theta_m) + f_1(\Theta_m)_{m+j}\delta_m^1$$

$$+ f_2(\Theta_m)_{m+j}\delta_m^2 + \cdots + f_{N-1}(\Theta_m)_{m+j}\delta_m^{N-1},$$

$$m = 1, M - j \qquad (15)$$

link $f(\theta)$ at the various measurement points to form a single smooth function over the range of the data. These equations are valid for values of j running from 1 to $N - 1$. A second set of auxiliary equations of the form

$$f_n(\Theta_{M+1-j}) = 0 \quad \text{if } n \geq j, \quad j = 1, N - 1 \qquad (16)$$

eliminate the higher-order derivatives of $f(\theta)$ for the large-angle data points where it is known to be very slowly varying.

The number of unknowns is

$$MN - \tfrac{1}{2}N(N-1).$$

These unknowns are contained in $MN - \tfrac{1}{2}N(N-1)$ linear coupled equations of the form of Eqs. (13) and (15). They are solved by standard numerical techniques to yield the apparatus–beam function $f(\theta)$ and its available derivatives at each measurement angle. The extracted differential cross sec-

tion $d\sigma_p/d\Omega$, at each measurement angle is found by multiplying this function by $ds_p/d\Omega$, as in Eq. (8).

For each data set, results are obtained for values of N ranging from 2 to 6. At each value of N, the calculated $d\sigma_p/d\Omega$ is convoluted with the incident-beam distribution and the detection-window width and a self-consistency confidence level determined for each data point. The value of N yielding a satisfactory confidence level depends on the angular width of the scattered-beam distribution and thus ranges from 3 or 4 for lower-energy data to 5 or 6 for the more sharply peaked high-energy measurements. Figure 4 displays the scaled $dI/d\Omega$, $ds_p/d\Omega$, and $d\sigma_p/d\Omega$ determined by the extraction method for a single angular acquisition of 100-keV-proton excitation of the $n=2$ level of helium. The brackets on $ds_p/d\Omega$ represent the confidence level of the calculation. The 100-keV data were chosen for this figure because the distorting effects of the incident-beam distribution and finite detection-window width are largest where the measured angular distribution is most sharply peaked. Thus, this data provides the most rigorous test of the extraction method. In laboratory units, the FWHM of the $dI/d\Omega$, $ds_p/d\Omega$ and $d\sigma_p/d\Omega$ are 126, 153, and 90 μrad, respectively. Note that at $\theta=0$, $d\sigma_p/d\Omega$ is twice as large as $ds_p/d\Omega$. Yet the standard deviation of the average of all of the 100 keV, $\theta=0$ results is only 40%.

The real power of the extraction scheme lies in the fact that it is linear but does not require specification of a functional form for $f(\theta)$ or $d\sigma_p/d\Omega$.
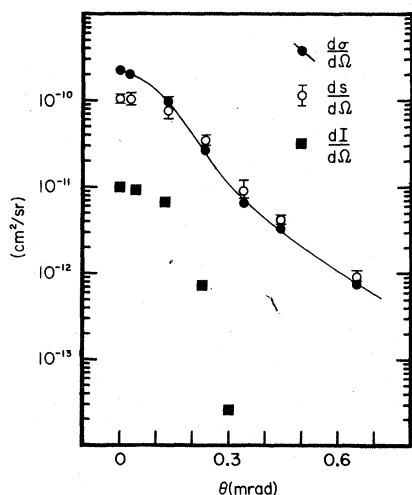

FIG. 4. Angular differential cross section for 100-keV-proton excitation of helium to the $n=2$ as determined from a single angular-spectrum measurement. $d\sigma/d\Omega$, derived angular differential cross section; $ds/d\Omega$, apparent angular differential cross section; $dI/d\Omega$, incident-beam angular distribution in arbitrary units.

Because the method is linear, it avoids problems associated with iterative schemes and reduces calculation time. Validity of the key assumption and convergence of the Taylor-series expansions are easily tested.

The obvious weakness of the method is the introduction of the approximations of the form of Eq. (16). If the angular measurements do not extend into the range where distortion due to beam and detection-window widths is small, the resulting $d\sigma_p/d\Omega$ could be severely affected at larger angles. However, even in the case of the exhibited data where the range of measurement was very small, $f(\theta)$ differed appreciably from a constant value only at very small angles. Furthermore, errors resulting from these approximations are shown to be small by comparing the measured and integrated $ds_p/d\Omega$.

Other methods of extracting the $d\sigma_p/d\Omega$ from Eq. (7) using iterative approximation techniques were studied and tested. In general, these methods required excessive computation time and were overly sensitive to normal statistical fluctuations in the data. Still other methods involving a linear or a nonlinear least-squares fitting of $f(\theta)$ to an assumed analytical form were similarly unsuccessful. An analytical form for $f(\theta)$ appropriate for all available data was never found. In cases where the results of these other methods could be compared to the results of the method discussed, the agreement was good.

IV. RESULTS AND DISCUSSION

The bombardment of helium by proton impact is one of the most thoroughly studied of all the collisional systems. Experimentally, helium is easy to handle. The availability of accurate theoretical transition probabilities for helium permits the emission cross sections to be converted to excitation cross sections. Total cross sections for excitation of helium by proton impact to all the helium singlet states through $n=6$ have been measured. In spite of these experimental advantages, the problems of measurement of excitation cross sections for the $n=2$ level in the 15–150-keV impact energy range are severe. The experimental studies of total cross sections for excitation of the $n=2$ level are limited to those of Park and Schowengerdt[5] and Hippler and Schartner.[6] There have been no previous measurements of angular differential cross sections for proton excitation of helium to any level.

Figure 5 shows angular differential cross sections obtained using the experimental technique and data-analysis method discussed above. Cross sections for 25, 50, and 100 keV incident protons
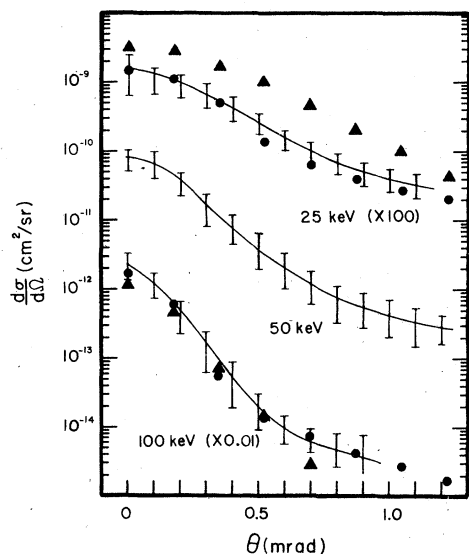
FIG. 5. Angular differential cross section for proton excitation of helium to the $n = 2$ state. Data, —; theory, Flannery and McCann, Ref. 10, four-state eikonal, ●; Born approximation, ▲.

for the process $H^+ + He(1\,^1S) \rightarrow H^+(\theta) + He^*(n = 2)$ are shown. The error bars shown are one rms deviation obtained from averaging the extracted $d\sigma_p/d\Omega$. No estimate of possible systematic error is included.

The largest potential source of systematic error is the data-analysis method; specifically, the first assumption and the auxiliary equations of the form Eq. (16). In addition, systematic error may arise from the absolute measurement of the interaction length and pressure. The interaction length is determined after assembling the collision chamber by measuring the distance between marks scribed on the outer walls of the chamber during its construction. Because of the long time required to complete a sequence of data acquisition, the value of $(I_0)_f$ corresponding to a specific angular measurement of $I_p(\theta)$ is more uncertain than is the angular distribution. This means that the shape of the curve is more reliable than the absolute magnitude. This is illustrated by the fact that the random error bars are of essentially constant magnitude over the entire angular range. The Born calculations and the four-state eikonal calculations of Flannery and McCann[10] are also shown in Fig. 5. The agreement with the four-state eikonal calculation in both curve shape and absolute magnitude is unexpectedly good at both 25 and 100 keV. The theoretical calculations are a sum of the contributions from the $2\,^1S$ and $2\,^1P$ states only. However, this does not affect the comparison with experiment because the contribution from the triplet states is negligible due to spin conservation. In
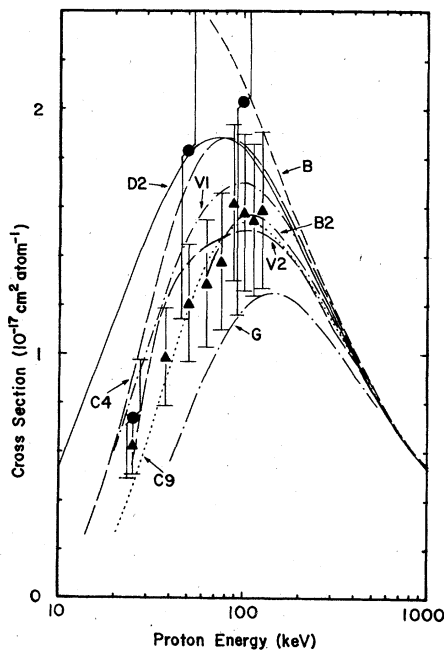

FIG. 6. Total excitation cross sections for the process $H^+ + He(1\,^1S) \rightarrow H^+ + He(2\,^1S + 2\,^1P)$. ●, present results. ▲, Park and Schowengerdt, Ref. 5. Curve B: Born, Bell et al., Refs. 11 and 12. Curve B2: second Born, Holt et al., Ref. 13. Curve C4: four-state close coupling, Flannery, Ref. 14. Curve C9: nine-state close coupling, Van den Bos, Ref. 15. Curve D2: second-order diagonalization, Baye and Heenen, Ref. 17. Curve V1: first-order potential, Joachain and Vanderpoorten, Ref. 16. Curve V2: second-order potential, Begum et al., Ref. 18. Curve G: Glauber, Joachain, and Vanderpoorten, Ref. 16.

the experiment, all of the $n = 2$ states are included in the measurement and the substates are not distinguished. At 25 keV, the Born calculation lies above the experimental results at the angles shown. At 100 keV, the Born results do as well as the four-state eikonal calculation of Flannery and McCann at the small angles, but they cross over the experimental results around 0.5 mrad and decrease quite rapidly thereafter. This illustrates that the total cross sections of two different theories may be in reasonable agreement while their differential cross sections are vastly different. Thus, the angular differential cross section provides a much stronger test for any theoretical calculation.

Total cross sections for the process $H^+ + He \rightarrow H^+ + He^*$ $(n = 2)$ can be obtained from the differential cross sections by numerical integration. In Fig. 6, the results obtained by this method are compared to the experimental results of Park and Schowengerdt[5] and various theoretical results.[11-18] The integration of the differential cross section to give the total cross section $\sigma = 2\pi \int (d\sigma/d\Omega) \sin\theta \, d\theta$ tends to emphasize the contribution of the large-

angle measurements which are the most uncertain. As noted above, errors in absolute magnitude are also more likely in the differential measurements because of the long times required for data acquisition.

The total cross sections obtained by integration are shown only for comparison with the earlier results and cannot be expected to improve the accuracy of the measurements of Park and Schowengerdt.[5] The error bars representing the random errors of the current data overlap the earlier measurement of Park and Schowengerdt.[5] Considering the differences in technique, the agreement between the total cross section obtained by integrating the present results and the earlier total cross section measurement of Park and Schowengerdt[5] is quite acceptable.

Several calculations of the $H^+ + He \rightarrow H^+ + He^*$ $(n = 2)$ total cross section are available. Some of these calculations[11-18] are shown in Fig. 6. The uncertainty in the present data does not permit a choice between the various calculations. A remeasurement of the total cross section using improved techniques[1] would assist in evaluating the various theoretical calculations of total cross sections.

The excellent agreement of the present differential-cross-section measurements with the four-state eikonal calculation of Flannery and McCann[10] is perhaps fortuitous, especially with respect to magnitude. Additional collision systems will need to be studied to determine the limits on the validity of the approximations employed in the Flannery and McCann calculation. Chan and Chang[19] have calculated the differential cross section in the Glauber approximation for the excitation of the $2\,^1P$ state of helium by proton impact. However, they did not include the $2\,^1S$ state in their calculation so that the Glauber approximation cannot be compared with the experimental results obtained here. Additional theoretical calculations of the differential cross section for $H^+ + He \rightarrow H^*(\theta) + He^*$ $(n = 2)$ would aid in evaluating both the experimental results and the limitations of the approximations themselves.

[1]J. T. Park, in *Collision Spectroscopy*, edited by R. G. Cooks (Plenum, New York, 1978).

[2]J. T. Park, V. Pol, J. Lawler, and J. George, Phys. Rev. Lett. 30, 1013 (1973).

[3]V. Pol, W. Kauppila, and J. T. Park, Phys. Rev. A 8, 2990 (1973).

[4]J. T. Park, V. Pol, J. M. George, J. L. Parker, and J. L. Peacher, Phys. Rev. A 11, 857 (1975).

[5]J. T. Park and F. D. Schowengerdt, Phys. Rev. 185, 152 (1969).

[6]R. Hippler and K. H. Schartner, J. Phys. B 7, 618 (1974).

[7]J. T. Park and F. D. Schowengerdt, Rev. Sci. Instrum. 40, 753 (1969).

[8]G. W. York, Jr., J. T. Park, J. J. Miskinis, D. H. Crandall, and V. Pol, Rev. Sci. Instrum. 43, 230 (1972).

[9]V. Pol, W. Kauppila, and J. T. Park, Phys. Rev. A 8,

2990 (1973).

[10]M. R. Flannery and K. J. McCann, J. Phys. B 7, 1558 (1974).

[11]K. L. Bell, D. J. Kennedy, and A. E. Kingston, J. Phys. B 1, 1037 (1968).

[12]K. L. Bell, D. J. Kennedy, and A. E. Kingston, J. Phys. B 1, 218 (1968).

[13]A. R. Holt, J. Hunt, and B. L. Moiseiwitsch, J. Phys. B 4, 1318 (1971).

[14]M. R. Flannery, J. Phys. B 3, 305 (1970).

[15]J. van den Bos, Phys. Rev. 181, 191 (1969).

[16]C. J. Joachain and R. Vanderpoorten, J. Phys. B 7, 817 (1974).

[17]D. Baye and P. H. Heenen, J. Phys. B 6, 1255 (1973).

[18]S. Begum, B. H. Bransden, and J. Coleman, J. Phys. B 6, 837 (1973).

[19]F. T. Chan and C. H. Chang, Phys. Rev. A 11, 1097 (1975).